PAPER

Reorientation mechanisms of block copolymer/ CdSe quantum dot composites under application of an electric field†

Christine C. Kathrein,[a] Christian Pester,[b] Markus Ruppel,[c] Maike Jung,[a] Marc Zimmermann[c] and Alexander Böker*[c]

Time- and temperature-resolved *in situ* birefringence measurements were applied to analyze the effect of nanoparticles on the electric field-induced alignment of a microphase separated solution of poly(styrene)-*block*-poly(isoprene) in toluene. Through the incorporation of isoprene-confined CdSe quantum dots the reorientation behavior is altered. Particle loading lowers the order–disorder transition temperature, and increases the defect density, favoring nucleation and growth as an alignment mechanism over rotation of grains. The temperature dependent alteration in the reorientation mechanism is analyzed *via* a combination of birefringence and synchrotron SAXS. The detailed understanding of the effect of nanoparticles on the reorientation mechanism is an important prerequisite for optimization of electric-field-induced alignment of block copolymer/nanoparticle composites where the block copolymer guides the nanoparticle self-assembly into anisotropic structures.

1 Introduction

Approaching the nanometer length scale, classical photo lithographic methods reach their limits, and self-assembly processes are becoming a promising and cost-efficient alternative. In particular, block copolymer/nanoparticle composite materials have gained considerable interest in the past decade due to their wide variety of potential applications. While the nanoparticles exhibit interesting catalytic,[1] optical,[2–4] mechanical,[3] or magnetic properties,[5] block copolymers, can effectively control particle location and patterns.[6,7] Utilizations include photonic band gap materials,[7,8] solar cells,[9] and catalytic[1] and biomedical devices.[10]

The properties of the composite materials are not only determined by particle size and shape, but also by the spatial distribution within the polymer matrix. Therefore, precise control over the particle assembly and orientation is required. Block copolymers, which are capable of forming a rich variety of structures in a size range of 10–100 nm, are the ideal scaffold for the assembly. Through selective insertion into one block copolymer domain, highly ordered arrays of nanoparticles are producible. The crucial parameter determining the affinity to the individual block copolymer constituents is the chemical surface modification of the particle.[11] The localization within the domain is mainly influenced by its core diameter and the grafting densities and molecular weights of the ligands.[12]

If no directing patterns or orienting stimuli are applied, the block copolymers form an isotropic multidomain structure. However, for most applications precise control over orientation with a minimum amount of defects is favorable. Different techniques have been established to obtain highly aligned samples from block copolymers, for example the application of external stimuli such as magnetic[13,14] or electric fields,[15] shear force,[16,17] temperature gradients,[18] and patterned substrates[19–21] have been thoroughly investigated.

Foundation of the realignment process under application of an electric field is the difference in dielectric permittivity $\Delta\varepsilon = \varepsilon_A - \varepsilon_B$ between the copolymer blocks. Dielectric interfaces perpendicular to the electric field vector are electrostatically unfavorable compared to those parallel to the external field. The energy difference between the two orientations is proportional to the second power of the dielectric contrast $(\Delta\varepsilon)^2/\bar{\varepsilon}$ between the two blocks devided by the mean dielectric permittivity of the sample.[22] To obtain the energetically favorable orientation with interfaces parallel to the electric field vector, block copolymers can undergo three different microscopic

[a] DWI – Leibniz Institut für Interaktive Materialien, Institut für Physikalische Chemie, RWTH Aachen University D-52062 Aachen, Germany

[b] University of California, Materials Research Laboratory, Santa Barbara, CA, 93106, USA

[c] Fraunhofer-Institut für Angewandte Polymerforschung – IAP, Lehrstuhl für Polymer-materialien und Polymertechnologie, Universität Potsdam, D-14476 Potsdam-Golm, Germany. E-mail: alexander.boeker@iap.fraunhofer.de; Fax: +49 (0) 331/568 3000; Tel: +49 (0) 331/568 1112

mechanisms of alignment: nucleation and growth (NG), rotation of grains (RG),[23,24] and selective disordering (SD). Which mechanism is exploited strongly depends on the temperature and preorientation of the sample. Selective disordering is merely found in close vicinity to the order–disorder transition temperature T_{ODT} and therefore will not be discussed in this publication. For a detailed explanation the authors refer to an article by Ruppel *et al.*[25] A precise description of the two other reorientation mechanisms will be given in the course of this publication.

Although much effort has been given to understand the effects of electric fields on the block copolymer microstructure,[26–29] only few studies exist on how nanoparticles influence the electric field-induced alignment. Cell dynamic system simulations by Yan and coworkers revealed that the nanoparticles alter the morphology and reorientation dynamics of block copolymers under the influence of electric fields.[30] Furthermore, Yan *et al.* anticipated that the inclusion of nanoparticles leads to an alteration in alignment mechanism with a preference of NG over RG.[31] Liedel *et al.* showed that selectively-confined gold nanoparticles lower the critical field strength necessary to align poly(styrene)-*block*-poly(2-vinylpyridine) thin films.[32]

In this publication the electric field-driven alignment of microphase separated polystyrene-*block*-polyisoprene solutions with polyisoprene-confined oleylamine-capped CdSe nanoparticles (CdSe-Np) is investigated by means of a combination of birefringence and *in situ* synchrotron small-angle X-ray scattering. In the past birefringence measurements have been utilized to analyze the alignment of block copolymers under shear flow.[33–35] Chen *et al.* proposed a combination of *in situ* rheo-optical measurements, *ex situ* electron microscopy and *in situ* SAXS to probe alterations in microstructure and orientation upon flow-induced alignment.[36] Birefringence measurements offer excellent time resolution while providing information on the degree of alignment of optically anisotropic block copolymer microstructures and are therefore well suitable for the real-time analysis of the alignment kinetics.

We demonstrate that nanoparticles are capable of switching the reorientation mechanism of electric field-induced alignment as anticipated by Yan and coworkers. Poly(styrene)-*block*-poly-(isoprene) (SI) (33.2 wt%) in toluene was chosen as a model system due to the fact that its alignment kinetics and reorientation mechanisms under exposure to an electric field have been intensively analyzed *via* synchrotron small angle X-ray scattering (SAXS).[23,37] Therefore, the comparison to previously performed experiments is straightforward. Oleylamine functionalized CdSe quantum dots were incorporated into the lamella-forming block copolymer. Previous work with polystyrene-*block*-polyisoprene nanofibers revealed that the oleylligands of the particles are selectively confined within the polyisoprene phase.[38]

2 Materials and methods

2.1 Sample preparation

Lamella forming poly(styrene)-*block*-poly(isoprene) of a molecular weight of 108 kg mol^{-1} and a polydispersity index of 1.05 was synthesized by sequential living anionic polymerization. The volume fraction of the poly(styrene) block amounts 0.42 ($S_{42}I_{58}^{108}$). 33.2 wt% solutions of the block copolymer in the non-selective good solvent toluene were prepared. Oleylamine-stabilzed CdSe quantum dots with a peak emission at 525 nm and a particle diameter of 2.8 nm in hexane solution were purchased from STREM Chemicals Inc. The quantum dots were chosen since they show no absorption at the wavelength of the laser beam (λ = 632.8 nm). Through addition of twice the amount of ethanol absolute to the particle solution the quantum dots precipitated. Subsequently, the mixture was centrifuged at 11 000 rpm for 10 min. The hexane/ethanol mixture was decanted and the particles were dried under high vacuum for 2 hours. Afterwards, the quantum dots were dissolved in toluene which was then given to the block copolymer to attain concentrated solutions with a polymer concentration of 33.2 wt% and nanoparticle loadings of 0 wt%, 1 wt%, 2 wt%, and 3 wt% with respect to the amount of polymer.

2.2 Birefringence measurement system and sample cell

Time- and temperature-resolved *in situ* birefringence measurements are conducted with an Exicor 150AT from Hinds Instruments which measures magnitude (δ) and fast axis orientation of the sample's optical retardation with high accuracy (0.01 nm) and time resolution allowing the acquisition of up to three data points a second. Owing to its special design moving parts in the optical train can be avoided and the alteration of measurement angles is not necessary. The HeNe laser beam is first polarized by a 45° polarizer and subsequently passes through a photo elastic modulator (PEM). After traversing through the sample the beam is divided in two parts by a beam splitting mirror. Both beams afterwards pass through an analyzer, an optical filter, and a photodetector. A lock-in amplifier processes the electronic signals which are further converted using a software algorithm to determine the magnitude of retardation and the angle of fast axis orientation. The sample cell used for the measurements is presented in Fig. 1. The electric field was applied in a home-built capacitor in which the block copolymer solution was sandwiched between two gold electrodes ④ of a length of 1.5 cm with an electrode spacing of 2 mm and a path length of light of 5 mm. The laser beam with a diameter of 1 mm and a wavelength of 632.8 nm propagated through the solution directly between the gold electrodes perpendicular to the electric field vector. Measurements were performed in the middle of the capacitor to avoid any influence by fringe fields close to the electrode edges. Above and below the capacitor, two glass slides ⑨ prevented solvent evaporation which were tightly screwed to the sample cell. For SAXS measurements the glass slides can be exchanged by kapton sheets covered with a thin layer of teflon ⑧. Teflon pieces with the same dimensions as the glass slides (thickness: 1 mm; diameter: 3 cm) and a 1 mm wide centered hole directly above the middle of the capacitor, are pressed to the kapton sheets and screwed to the sample cell. This on the one hand fixes the kapton and on the other hand prevents voltage breakthrough to the outside of the cell. The temperature of the sample was precisely controlled using a circular Peltier element ⑦ which was placed directly underneath
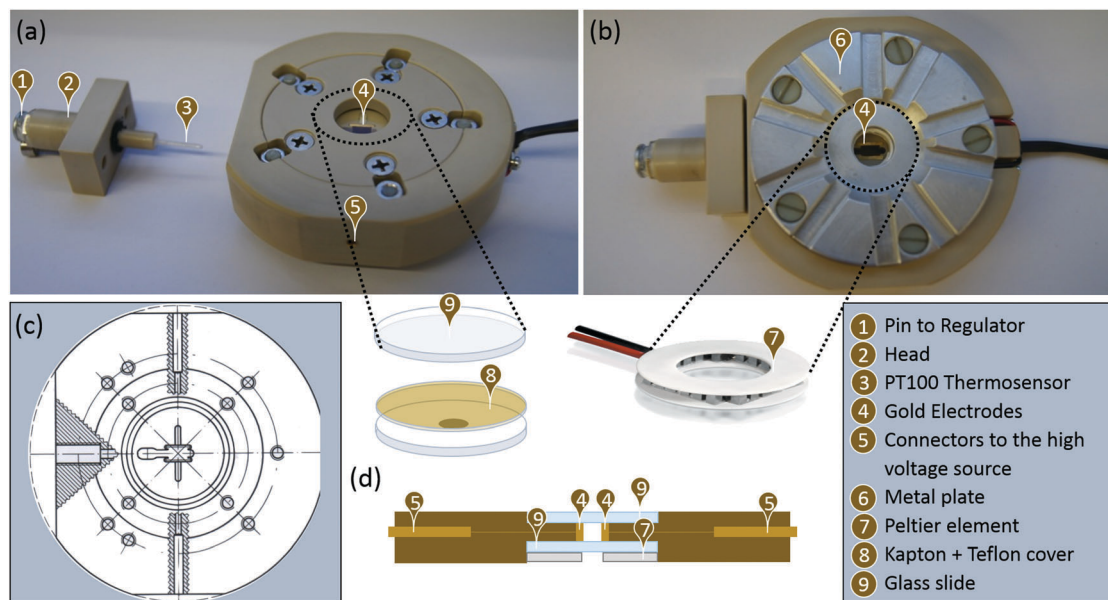
Fig. 1 (a and b) Photos of the sample cell used for the bulk analysis of block copolymers under the application of electric field. The block copolymer solution is sandwiched between two polished gold electrodes ④. Two glass slides ⑨ tightly seal the chamber above and below the parallel plate capacitor preventing solvent evaporation as demonstrated in the schematic cross section image (d). Heating- and cooling rates can precisely be regulated *via* a circular Peltier element ⑦. A metal plate ⑥ below the Peltier element ensures rapid heat transfer to the surrounding. The Head ② which seals the sample cell comprises a tiny PT100 thermosensor covered by thin glass ③ for precise *in situ* temperature determination. The high voltage power source is connected to the gold electrodes *via* ⑤. (c) Engineering drawing of the sample cell.

the capacitor. Additionally, the temperature was monitored in solution *via* a PT-100 thermosensor ③ covered with thin glass. To prevent solvent degradation of the sample cell, this was built from polyether ether ketone (PEEK).

2.3 Determination of the reorientational time constants *via* birefringence

The sample was heated to 10 °C above the T_{ODT} and subsequently cooled to 10 °C below the T_{ODT} at a heating and cooling rate of 1 °C min^{-1}. While the lamella phase is characterized by a strong degree of form birefringence, the disordered phase is optically isotropic. Therefore, the T_{ODT} can be determined by monitoring the decrease in phase retardation as a function of temperature. Afterwards, the block copolymer solution was quickly adjusted to the desired temperature. After cooling, the sample exhibits a microphase separated, isotropic multidomain structure with no preferred direction of orientation. Upon application of an electric field of 1 kV mm^{-1}, the increase in phase retardation is measured as a function of time. The data was fitted by a single exponential function to retrieve the overall reorientational time constant τ.

3 Results and discussion

3.1 SAXS analysis of block copolymer reorientation mechanisms under application of an electric field

While birefringence measurements offer excellent time resolution to analyze the reorientation kinetics of uniaxial block copolymer phases, an additional measurement technique is needed to draw conclusions about the underlying mechanism of reorientation. Publications by our group focused on unveiling the reorientation mechanisms of solutions of polystyrene-*block*-polyisoprene in toluene when exposed to electric fields.[23,25] Since we use the same system for our measurements these findings can be exploited to interpret the birefringence measurements described in this publication. Hence, the most important findings are summarized below. As stated above electric field induced reorientation of block copolymer samples can proceed *via* three different mechanisms: Rotation of Grains (RG), Nucleation and Growth (NG), and Selective Disordering (SD).

Previously, the reorientation mechanisms were distinguished by analysis of the time-evolution of the azimuthal intensity distribution of small angle X-ray scattering (SAXS) images upon inception of the electric field. A precise description of the measurements relevant to our study performed by Böker *et al.* can be found in the ESI† (see Fig. S1).[23] An important result of the measurements mentioned above is that the exploited reorientation mechanism is determined by the temperature at which the electric-field-induced alignment takes place with respect to the order–disorder transition temperature (T_{ODT}).

Well below the T_{ODT}, at lower temperatures, RG is the prevailing mechanism.[23] In this case, the orientation of entire grains rotates as schematically demonstrated in Fig. 2(a). In the strong segregation limit (SSL), the average dimension of one region of coherence is larger and the formation of grain boundaries is thermodynamically unfavorable.[15] Therefore the reorientation does not proceed *via* NG in this regime.

Nucleation and Growth (Fig. 2(b)) proceeds *via* the formation of nuclei of lamella with an enthalpically preferred orientation
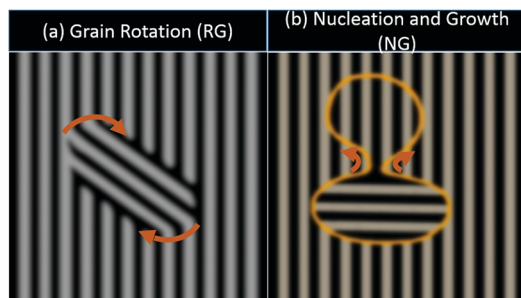
Fig. 2 Schematic image of possible reorientation mechanisms of block copolymers upon inception of electric fields: (a) Rotation of Grains (RG) and (b) Nucleation and Growth (NG).

parallel to the electric field vector and their subsequent growth. The starting point for the nucleation are defects, such as, for example, dislocations. NG is the prevailing mechanism at elevated temperatures, in the vicinity of the order–disorder transition, where the segregation between the blocks is weaker.[23] In this weak segregation limit (WSL), the energetic penalty induced by the creation of boundary interfaces is lower whereby small nuclei which have a large boundary area in comparison to their volume are more readily formed. Furthermore, this region is characterized by a higher defect density and mobility which also favors NG.

Compared to RG the reorientation through NG proceeds relatively slow whereby the time constants of reorientation at a given temperature can differ by an order of magnitude.[37]

Another important factor which greatly influences the reorientation of lamella domains under application of an electric field is the initial degree of order in the block copolymer sample. In misaligned samples, RG is the prevailing mechanism, while highly ordered block copolymers with lamella interfaces perpendicular to the electric field vector preferentially reorient *via* NG.[37] The boundary between the two mechanisms is not sharp; at medium conditions both can coexist. Therefore, conditions prior to realignment are crucial.

3.2 Analyzing block copolymer reorientation kinetics *via* birefringence

While all block copolymer phases posses intrinsic birefringence, form birefringence is limited to uniaxial block copolymer phases. Intrinsic birefringence results from the orientation of block end-to-end vectors, and the stretching of block copolymer chains away from the block–block interfaces. Lodge and Fredrickson predicted that the intrinsic birefringence is directly proportional to the stretching of the chains defined by $\frac{L^2}{\langle h^2 \rangle_0}$, where L is the layer thickness and $\langle h^2 \rangle_0$ is the mean-square unperturbed end-to-end distance.[39] In strongly segregated lamella and cylindrical block copolymer systems ($\chi N \gg 10$) this represents a significant contribution to the overall birefringence strength of the sample and can even be comparable to or greater than the form birefringence.[39] The interfaces separating the microdomains are very narrow since the system wants to

minimize the unfavorable A–B interfacial area. This results in perturbed, extended chain configurations and therefore in an entropic penalty. In our experiments the intrinsic birefringence of the block copolymer only has a minor contribution to the overall birefringence strength of the sample. The dilution of the polymer with toluene significantly lowers the T_{ODT} to 62.5 °C, hence the individual polymer chains are largely unperturbed. This assures sufficient mobility for the reorientation process. Fredrickson and Leibler demonstrated that the theoretical descriptions of block copolymers in the molten state can likewise be applied to block copolymers in nonselective good solvents.[40] In the following we will discuss how birefringence measurements can be utilized to analyze the reorientation kinetics of block copolymers as demonstrated by Amundson and coworkers.[41,42]

The polymer used in our study is characterized by a lamella microdomain structure. SAXS data of the exact same polymer in toluene solution can be found in previous publications by our group.[25] Ruppel *et al.* determined an order–disorder concentration of 28.5 wt% for the polymer ($S_{42}I_{58}^{108}$) in toluene solution at room temperature which is well below the concentration of 33.2 wt% used in our measurements. Fig. 3(a) displays a simplified illustration of a lamella stack, it's optic axis and the direction of the fast and the slow axis. A lamella microdomain pattern is characterized by a uniaxial optical anisotropy resulting in form birefringence. The axis of symmetry, also known as the optic axis, which is indicated by the green arrow in Fig. 3(a), is perpendicular to the lamella interfaces. Components of light propagating through the sample are exposed to different refractive indices n_o and n_e depending on whether their direction of polarization is perpendicular (ordinary wave (o), direction indicated by blue arrows) or parallel (extraordinary wave (e), direction indicated by red arrows) to the optic axis. In the case of negative uniaxial birefringence, as found in a lamella assembly, the fast axis coincides with the optic axis while the slow axis is perpendicular to it. Light polarized along the slow axis will be refracted with a refractive index n_o while light polarized along the fast axis is exposed to a refractive index n_e. Therefore, the ordinary wave will experience a phase retardation δ with respect to the
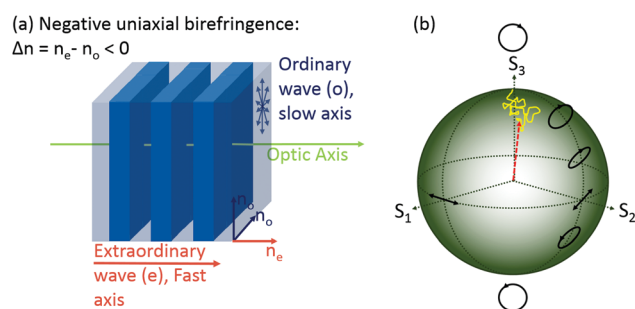

Fig. 3 (a) Simplified illustration of a single lamella stack, its optic axis and the direction of the slow and the fast axis with respect to the lamella interfaces. (b) Poincaré sphere. The change in polarization state of light of a monochromatic laser beam passing through a block copolymer sample can be described as a random walk on the poincaré sphere (here in yellow).

extraordinary wave.[43] The magnitude of the resulting phase retardation δ amounts to eqn (1).

$$\delta = 2\pi \frac{l}{\lambda} \Delta n^0 \langle \overline{\Psi^2} \rangle \sin^2 \theta \qquad (1)$$

here l is the optical path length, λ describes the wavelength of light while passing through the medium, $\langle \overline{\Psi} \rangle$ denotes the periodic lamella pattern, and θ is the angle between the propagation direction of light and the unit wave vector of the lamella pattern $\hat{e}_k$. $\Delta n = n_e - n_o$ is the birefringence of the sample. The overall birefringence strength of a block copolymer is dependent on its degree of phase separation. In the strong segregation limit (SSL) the interfaces are sharp and a maximum form birefringence strength Δn^0 is attained.[41]

Block copolymer samples comprise several grains. When no orienting stimuli are applied to the sample these grains are randomly oriented. In Fig. 4(a) the evolution of the phase retardation signal (δ) measured by the Exicor 150AT upon exposing a sample without quantum dots to an electric field of 1 kV mm^{-1} is plotted against time in seconds at three different temperatures. At the beginning of the measurement a phase retardation of around 0–10 nm is observed.

Prior to application of the electric field, the block copolymer sample was heated to 10 °C above the order–disorder transition temperature (T_{ODT} = 62.5 °C) at which the lamella microstructure disintegrates and approaches the disordered phase. Subsequently, the samples were cooled to 10 °C below T_{ODT} at a cooling rate of 1 °C min^{-1}. By heating the sample above the T_{ODT} and subsequent cooling into the phase separated state,

a macroscopically isotropic multidomain structure is generated with no preferred orientation as schematically demonstrated in Fig. 4(b). This ensures that the initial conditions of alignment are comparable at all temperatures and nanoparticle loadings. When light propagates through the sample, each region of coherence induces a small phase retardation depending on its size, degree of phase segregation, and orientation. Amundson et al.[41] described the propagation of light through a macroscopically disoriented sample as a random walk on the poincaré sphere – a spherical surface of unit diameter on which each point corresponds to a different polarization state of light.[41] A schematic image of the poincaré sphere is given in Fig. 3(b).

Upon passing through the sample each encounter of light with a grain can be described as a small change of position on the poincaré sphere, whereby direction and magnitude of the step are determined by the orientation, the birefringence strength and the size of the grain. This results in a series of uncorrelated small phase retardations. The associated trajectory on the poincaré sphere is exemplified in yellow in Fig. 3(b). The overall birefringent phase retardation is determined by the position of the end point.

The laser beam utilized in this study has a diameter of 1 mm while typical grain dimensions lie between 1 µm and 10 µm. Therefore, one ray of light traverses through various microstructural arrangements. The overall polarization state of the laser beam exiting the sample will be a mixed state composed of the individual end points of the random walks. Since these individual phase retardations are uncorrelated, in case of a macroscopically disordered sample the resulting overall δ is of low value.

After an electric field of 1 kV mm^{-1} was applied, the electric field-induced reorientation process set in and an increase in δ over time was observed. The degree of alignment of a block copolymer sample is described by the orientational order parameter P_2.

$$P_2 = \frac{3\langle \cos^2 \theta \rangle - 1}{2} \qquad (2)$$

A macroscopically disordered sample is characterized by $P_2 = 0$ (Fig. 4(b)) while a maximum alignment of lamella interfaces parallel to the electric field vector corresponds to an order parameter of $-1/2$ (Fig. 4(c)). For perfect alignment perpendicular to the electric field vector $P_2 = 1$ is found (Fig. 4(d)). The effective overall birefringence strength of the block copolymer sample composed of various small grains is directly proportional to the order parameter and amounts eqn (3).

$$\Delta n = \Delta n^0 \langle \overline{\Psi^2} \rangle P_2 \sin^2 \theta \qquad (3)$$

Therefore, the phase retardation can be used as a direct measure to analyze the reorientation kinetics. To retrieve the overall reorientational time constant τ the data was fitted by a single exponential function $\delta = \delta_\infty + Ae^{(-t/\tau)}$.

As can be observed in Fig. 4(a) the maximum δ values (δ_∞) differ from each other after application of the electric field. In Fig. S2 of the ESI† the δ_∞ values obtained from the fit functions are plotted against the alignment temperature. Between 40 °C and
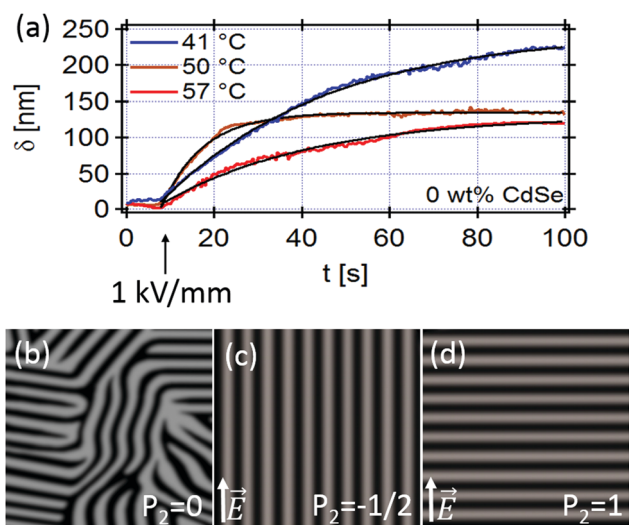

Fig. 4 (a) Evolution of phase retardation of a sample of poly(styrene)-block-poly(isoprene) (33.2 wt%) in toluene upon application of an electric field of 1 kV mm^{-1} at different temperatures. The wavelength of the laser beam used for the measurements amounts 632.8 nm. The phase retardation δ increases proportional to the order parameter of the sample. The data was fitted by a single exponential function (black line). (b and c) Schematic illustration of the lamella microstructure before (b) and after (c) electric field-induced alignment. (d) Schematic illustration of a lamella microstructure oriented perpendicular to the electric field vector. P_2 is the corresponding order parameter.

55 °C a decrease in δ_∞ is observed. This can be attributed to the less defined interfacial boundaries between the block copolymer constituents in the weak segregation limit (WSL). Hence, the maximum attainable form birefringence strength Δn^0 and therefore also δ_∞ decreases upon approaching the order–disorder transition temperature. Since the interfaces are less defined the dielectric contrast between the blocks, which is the main driving force for electric field induced alignment, likewise decreases with rising temperature. Hence, it is expected that also the absolute value of the maximum attainable P_2 is lowered. The two factors are interlinked. Therefore, we cannot distinguish to which percentage a decrease in δ_∞ is induced by a reduction of P_2 or Δn^0. Between 55 °C and 60 °C no further decrease in δ_∞ is observed, values fluctuate around 100 nm.

3.3 Analyzing the switch in reorientation mechanism *via* birefringence

The reorientation kinetics of the block copolymer sample without nanoparticles and with a nanoparticle loading of 1 wt% were analyzed *via* birefringence measurements at a field strength of 1 kV mm^{-1} in a temperature range between 30 °C and 60 °C. Owing to the intensive synchrotron SAXS studies on solutions of SI in toluene by Böker *et al.*[23] described above direct conclusions on the reorientation mechanisms can be drawn from the birefringence measurements. Furthermore, a detailed synchrotron SAXS study on the alignment mechanisms of $S_{42}I_{58}^{108}$ in toluene solution, which was also used for the measurements reported here, is described in a recent publication by our group and will be compared to our results in the course of the discussion.[25]

In the following, a description on how the switch in reorientation mechanism can be detected by birefringence measurements is given.

In Fig. 5 the determined reorientational time constants τ are plotted against the temperature for a sample with 0 wt% and 1 wt% CdSe nanoparticles. The reorientation kinetics are strongly dependent on the temperature of the sample.

At first we will focus our discussion on the development of the reorientational time constants with increasing temperature of the sample with 0 wt% nanoparticles (black squares Fig. 5). Between 28 °C and 50 °C τ decreases with rising temperature. In this low temperature regime all block copolymer domains reorient *via* RG.[23,25] Upon raising the temperature, chain mobility is enhanced while the viscosity of the sample is lowered, leading to a faster reorientation. As long as all grains realign *via* RG, a decrease in τ proportional to the increase in temperature is found as expected. The fact that the reorientational constant increases again upon further temperature elevation between 50 °C and 60 °C is most likely due to the onset of a slower realignment mechanism. According to previously published SAXS data NG sets in as an additional alignment mechanism in vicinity of the T_{ODT}.[23,25] Ruppel *et al.* analyzed a concentrated solution of $S_{42}I_{58}^{108}$ in toluene, the polymer also used in this study, at 2.6 K below T_{ODT}. When an electric field of 1 kV mm^{-1} was applied to the sample the polymer was shown to reorient *via* a pure nucleation and growth mechanism. Since Ruppel *et al.* used a toluene

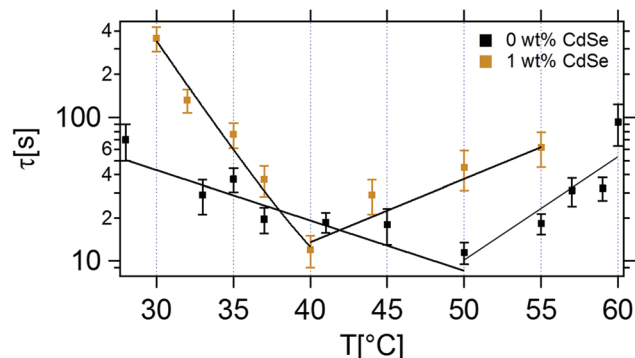**Fig. 5** Time constants of the electric field-induced reorientation at 1 kV mm^{-1} for a sample of poly(styrene)-*block*-poly(isoprene) (33.2 wt%) in toluene without nanoparticles (black squares) and with 1 wt% of CdSe quantum dots (orange squares) as a function of temperature.

solution of the same polymer, with the same initial prealignment, reoriented at the same electric field strength of 1 kV mm^{-1} the results can directly be compared to our birefringence data.

Fig. 5 shows that τ reaches a maximum value at 60 °C, which is 2.5 K below T_{ODT}. As described above the polymer reorients *via* a pure nucleation and growth mechanism at this temperature.[25] In a temperature range between 50 °C and 60 °C an increase in τ is observed with temperature. This can be explained by a coexistence of both mechanisms: with increasing temperature, the slower NG mechanism is increasingly preferred over RG. Since the percentage of grains realigned *via* NG increases with temperature, τ rises upon temperature elevation. Unfortunately, it is not possible to resolve the individual time constants of the two reorientation mechanisms since the two reorientation processes are interlinked.[37]

One might also interpret the slowing down of realignment kinetics with temperature between 50 °C and 60 °C as an effect of a simple reduction of dielectric contrast due to blurring of the boundary between the blocks in proximity of T_{ODT}.[13] This would lead to a reduced driving force for the reorientation process and hence to a worse overall alignment. To solve this issue we refer to Fig. S2 of the ESI,† where the maximum attainable birefringence retardation after realignment (δ_∞) is plotted *vs.* T. As stated above (δ_∞) is a measure of the order parameter after realignment and the degree of phase separation of the block copolymer. While (δ_∞) clearly decreases between 40 °C and 50 °C, no further decrease is observed in the temperature range in question. Hence, if the reduction of dielectric contrast should be reflected in a slowing down of realignment kinetics we would rather expect an increase in τ between 40 °C and 50 °C where according to Fig. 5 a clear decrease is observed. In the temperature range where an increase of τ is found, δ_∞ shows no clear trend with temperature and fluctuates around values of about 100 nm. Considering these observations and the information from the SAXS studies it is more probable that the slower alignment kinetics with rising temperature above 50 °C are induced by the onset of NG as an additional realignment mechanism.
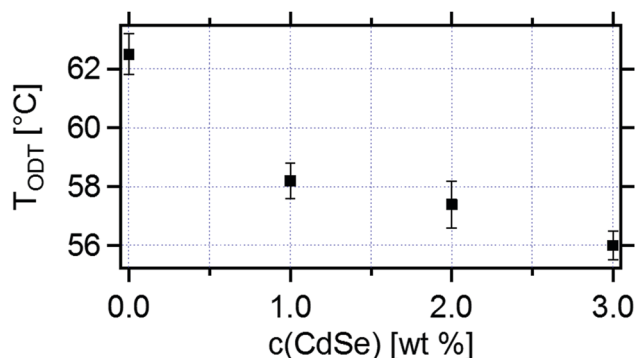
Fig. 6 Order–disorder transition temperature of a solution of SI (33.2 wt%) in toluene as a function of nanoparticle concentration. The poly(isoprene) confined CdSe quantum dots lower the order–disorder transition temperature of the sample.

3.4 The effect of nanoparticles on the reorientation mechanism and kinetics

Upon comparison of the measurements with (yellow squares Fig. 5) and without particles (black squares Fig. 5), it becomes apparent that a low nanoparticle amount (1 wt%) is already sufficient to lower the temperature at which NG sets in as an additional mechanism by 10 °C down to a temperature of 40 °C. The results presented here are the first experimental evidence that the reorientation behavior is altered through the confinement of quantum dots.

Two main factors are responsible for the onset of NG at lower temperatures upon addition of nanoparticles. On the one hand the incorporation of nanoparticles into block copolymers lowers the order–disorder transition temperature (T_{ODT}).[44] T_{ODT} of the samples was plotted against the quantum dot concentration (Fig. 6). At a nanoparticle loading of 1 wt% the T_{ODT} is lowered by 4.5 °C compared to the sample without particles. On the other hand nanoparticles increase the defect density in the block copolymer compared to the pure samples. The quantum dots serve as nuclei for their preferential phase and support the formation and coarsening of grains. The activation energy for the nucleation and growth process is decreased and NG becomes the thermodynamically preferred mechanism of realignment.[45]

4 Conclusion

In conclusion, *in situ* birefringence measurements were applied to analyze the influence of quantum dots on the reorientation behavior of block copolymers upon inception of an electric field of 1 kV mm^{-1}. The birefringence measurements have the advantage of being inexpensive and easily accessible while at the same time offering a high time resolution to monitor the reorientation processes. The data presented here gives the first experimental evidence that the incorporation of nanoparticles into block copolymers leads to a preference of NG over RG.

References

1 T. F. Jaramillo, S. H. Baeck, B. R. Cuenya and E. W. McFarland, *J. Am. Chem. Soc.*, 2003, **125**, 7148–7149.

2 M. Maldovan, A. Urbas, N. Yufa, W. Carter and E. Thomas, *Phys. Rev. B: Condens. Matter Mater. Phys.*, 2002, **65**, 165123.

3 G. A. Buxton, J. Y. Lee and A. C. Balazs, *Macromolecules*, 2003, **36**, 9631–9637.

4 M. Bockstaller and E. Thomas, *Phys. Rev. Lett.*, 2004, **93**, 166106.

5 S. Torquato, S. Hyun and A. Donev, *Phys. Rev. Lett.*, 2002, **89**, 266601.

6 R. B. Thompson, V. V. Grinzburg, M. W. Matsen and A. C. Balazs, *Science*, 2001, **292**, 2469.

7 R. B. Thompson, V. V. Grinzburg, M. W. Matsen and A. C. Balazs, *Macromolecules*, 2002, **35**, 1060.

8 A. J. A. Schultz, C. K. Hall, J. Genzer and N. Carolina, *Macromolecules*, 2005, **35**, 1060–1071.

9 W. U. Huynh, J. J. Dittmer and A. P. Alivisatos, *Science*, 2002, **295**, 2425–2427.

10 C. Kaittanis, S. A. Naser and J. M. Perez, *Nano Lett.*, 2007, **7**, 380–383.

11 J. J. Chiu, B. J. Kim, E. J. Kramer and D. J. Pine, *J. Am. Chem. Soc.*, 2005, **127**, 5036–5037.

12 M. R. Bockstaller, R. A. Mickiewicz and E. L. Thomas, *Adv. Mater.*, 2005, **17**, 1331–1349.

13 M. Gopinadhan, P. W. Majewski, Y. Choo and C. O. Osuji, *Phys. Rev. Lett.*, 2013, **110**, 078301.

14 Y. Rokhlenko, M. Gopinadhan, K. Zhang, C. S. O'Hern, R. Larson, P. Gopalan, P. W. Majewski, K. G. Yager and C. O. Osuji, *Phys. Rev. Lett.*, 2015, **115**, 258302.

15 K. Amundson, E. Helfand, D. D. Davis, X. Quan, S. S. Patel and S. D. Smith, *Macromolecules*, 1991, **24**, 6546–6548.

16 Z. R. Chen, J. A. Kornfield, S. D. Smith, J. T. Grothaus and M. M. Satkowski, *Science*, 1997, **277**, 1248–1253.

17 A. Keller, E. Pedemonte and F. M. Willmouth, *Nature*, 1970, **225**, 538–539.

18 B. C. Berry, A. W. Bosse, J. F. Douglas, R. L. Jones and A. Karim, *Nano Lett.*, 2007, **7**, 2789–2794.

19 I. Bita, J. K. Yang, Y. S. Jung, C. A. Ross, E. L. Thomas and K. K. Berggren, *Science*, 2008, **321**, 939–943.

20 R. A. Segalman, H. Yokoyama and E. J. Kramer, *Adv. Mater.*, 2010, **104**, 1152–1155.

21 R. Ruiz, H. Kang, F. A. Detcheverry, E. Dobisz, D. S. Kercher, T. R. Albrecht, J. J. Pablo and P. F. Nealey, *Science*, 2008, **321**, 936–939.

22 Y. Tsori, *Rev. Mod. Phys.*, 2009, **81**, 1471–1494.

23 A. Böker, H. Elbs, H. Hänsel, A. Knoll, S. Ludwigs, H. Zettl, V. Urban, V. Abetz, A. H. E. Müller and G. Krausch, *Phys. Rev. Lett.*, 2002, **89**, 135502.

24 M. Pinna, L. Schreier and A. V. Zvelindovsky, *Soft Matter*, 2009, **5**, 970–973.

25 M. Ruppel, C. W. Pester, K. M. Langner, G. J. A. Sevink, H. G. Schoberth, K. Schmidt, V. S. Urban, J. W. Mays and A. Böker, *ACS Nano*, 2013, **7**, 3854–3867.

26 C. W. Pester, M. Ruppel, H. G. Schoberth, K. Schmidt, C. Liedel, P. van Rijn, K. A. Schindler, S. Hiltl, T. Czubak, J. Mays, V. S. Urban and A. Böker, *Adv. Mater.*, 2011, **23**, 4047–4052.

27 A. Böker, H. Elbs, H. Hänsel, A. Knoll, S. Ludwigs, H. Zettl, A. V. Zvelindovsky, G. J. A. Sevink, V. Urban, V. Abetz, A. H. E. Müller and G. Krausch, *Macromolecules*, 2003, **36**, 8078–8087.

28 K. Schmidt, H. G. Schoberth, M. Ruppel, H. Zettl, H. Hänsel, T. M. Weiss, V. Urban, G. Krausch and A. Böker, *Nat. Mater.*, 2008, **7**, 142–145.

29 C. Liedel, C. W. Pester, M. Ruppel, C. Lewin, M. J. Pavan, V. S. Urban, R. Shenhar, P. Bösecke and A. Böker, *ACS Macro Lett.*, 2012, **2**, 53–58.

30 L.-T. Yan, H. G. Schoberth and A. Böker, *Soft Matter*, 2010, **6**, 5956–5964.

31 L.-T. Yan, H. G. Schoberth and A. Böker, *Macromol. Chem. Phys.*, 2009, **210**, 1003–1010.

32 C. Liedel, K. A. Schindler, M. J. Pavan, C. Lewin, C. W. Pester, M. Ruppel, V. S. Urban, R. Shenhar and A. Böker, *Small*, 2013, **9**, 3276–3281.

33 V. K. Gupta, R. Krishnamoorti, Z.-R. Chen and J. A. Kornfield, *Macromolecules*, 1996, **29**, 875–884.

34 V. K. Gupta, R. Krishnamoorti, J. A. Kornfield and S. D. Smith, *Macromolecules*, 1995, **28**, 4464–4474.

35 H. Wang, M. C. Newstein, M. Y. Chang, N. P. Balsara and B. A. Garetz, *Macromolecules*, 2000, **33**, 4185–4195.

36 Z.-R. Chen and J. A. Kornfield, *Polymer*, 1998, **39**, 4679–4699.

37 K. Schmidt, A. Böker, H. Zettl, F. Schubert, H. Hänsel, F. Fischer, T. M. Weiss, V. Abetz, A. V. Zvelindovsky, G. J. A. Sevink and G. Krausch, *Langmuir*, 2005, **21**, 11974–11980.

38 V. Kalra, J. Lee, J. H. Lee, S. G. Lee, M. Marquez, U. Wiesner and Y. L. Joo, *Small*, 2008, **4**, 2067–2073.

39 T. P. Lodge and G. H. Fredrickson, *Macromolecules*, 1992, **25**, 5643–5650.

40 G. H. Fredrickson and L. Leibler, *Macromolecules*, 1989, **22**, 1238–1250.

41 K. Amundson, E. Helfand, S. S. Patel and X. Quan, *Macromolecules*, 1992, **25**, 1935–1940.

42 K. Amundson, E. Helfand, X. Quan and S. D. Smith, *Macromolecules*, 1993, **26**, 2698–2703.

43 M. Born and E. Wolf, *Principal of optics: electromagnetic theory of propagation interference and diffraction of light*, Cambridge University Press, 1959.

44 A. Jain, J. S. Gutmann, C. B. W. Garcia, Y. Zhang, M. W. Tate, S. M. Gruner and U. Wiesner, *Macromolecules*, 2002, **35**, 4862–4865.

45 A. V. Zvelindovsky and G. J. A. Sevink, *Phys. Rev. Lett.*, 2003, **90**, 49601.